Detection of lipid in atherosclerotic vessels using ultrasound-guided spectroscopic intravascular photoacoustic imaging

Bo Wang,[1] Jimmy L. Su,[1] James Amirian,[2] Silvio H. Litovsky,[3] Richard Smalling,[2] Stanislav Emelianov[1,*]

[1]*Department of Biomedical Engineering, University of Texas at Austin, Austin, TX, 78712, USA*
[2] *Division of Cardiology, University of Texas Health Science Center, Houston, TX 77030 USA*
[3] *Department of Pathology, University of Alabama Birmingham, Birmingham, AL 35249 USA*
**emelian@mail.utexas.edu*

Abstract: Lipid is a common constituent in atherosclerotic plaques. The location and area of the lipid region is closely related to the progression of the disease. Intravascular photoacoustic (IVPA) imaging, a minimally invasive imaging modality, can spatially resolve the optical absorption property of arterial tissue. Based on the distinct optical absorption spectrum of fat in the near infrared wavelength range, spectroscopic IVPA imaging may distinguish lipid from other water-based tissue types in the atherosclerotic artery. In this study, a bench-top spectroscopic IVPA imaging system was used to ex-vivo image both atherosclerotic and normal rabbit aortas. By combing the spectroscopic IVPA image with the intravascular ultrasound (IVUS) image, lipid regions in the aorta were identified. The results demonstrated that IVUS-guided spectroscopic IVPA imaging is a promising tool to differentiate lipid in atherosclerosis.

OCIS codes: (110.5120) Photoacoustic imaging; (110.7170) Ultrasound; (170.0170) Medical optics and biotechnology; (170.6510) Spectroscopy, tissue diagnostics; (170.6935) Tissue characterization.

References and links

1. D. Lloyd-Jones, R. Adams, M. Carnethon, G. De Simone, T. B. Ferguson, K. Flegal, E. Ford, K. Furie, A. Go, and K. Greenlund, "Heart disease and stroke statistics-2009 update. A report from the American Heart Association statistics committee and stroke statistics subcommittee," Circulation (2008).
2. J. Sanz, and Z. A. Fayad, "Imaging of atherosclerotic cardiovascular disease," Nature **451**(7181), 953–957 (2008).
3. E. Falk, "Pathogenesis of atherosclerosis," J. Am. Coll. Cardiol. **47**(8 Suppl), C7–C12 (2006).
4. D. Vela, L. M. Buja, M. Madjid, A. Burke, M. Naghavi, J. T. Willerson, S. W. Casscells, and S. Litovsky, "The role of periadventitial fat in atherosclerosis," Arch. Pathol. Lab. Med. **131**(3), 481–487 (2007).
5. S. Tsimikas, B. P. Shortal, J. L. Witztum, and W. Palinski, "In vivo uptake of radiolabeled MDA2, an oxidation-specific monoclonal antibody, provides an accurate measure of atherosclerotic lesions rich in oxidized LDL and is highly sensitive to their regression," Arterioscler. Thromb. Vasc. Biol. **20**(3), 689–697 (2000).
6. B. D. MacNeill, H. C. Lowe, M. Takano, V. Fuster, and I. K. Jang, "Intravascular modalities for detection of vulnerable plaque: current status," Arterioscler. Thromb. Vasc. Biol. **23**(8), 1333–1342 (2003).
7. S. Sethuraman, S. R. Aglyamov, J. H. Amirian, R. W. Smalling, and S. Y. Emelianov, "Intravascular photoacoustic imaging using an IVUS imaging catheter," IEEE Trans. Ultrason. Ferroelectr. Freq. Control **54**(5), 978–986 (2007).
8. A. A. Oraevsky, and A. A. Karabutov, *Optoacoustic tomography*, Biomedical Photonics Handbook (CRC Press, 2003), Vol. 34, pp. 1–34.
9. S. Sethuraman, J. H. Amirian, S. H. Litovsky, R. W. Smalling, and S. Y. Emelianov, "Spectroscopic intravascular photoacoustic imaging to differentiate atherosclerotic plaques," Opt. Express **16**(5), 3362–3367 (2008).
10. B. Wang, E. Yantsen, T. Larson, A. B. Karpiouk, S. Sethuraman, J. L. Su, K. Sokolov, and S. Y. Emelianov, "Plasmonic intravascular photoacoustic imaging for detection of macrophages in atherosclerotic plaques," Nano Lett. **9**(6), 2212–2217 (2009).
11. S. Emelianov, S. Aglyamov, J. Shah, S. Sethuraman, W. Scott, R. Schmitt, M. Motamedi, A. Karpiouk, and A. Oraevsky, "Combined ultrasound, optoacoustic, and elasticity imaging," Proc. SPIE **5320**, 101–112 (2004).

#121713 - $15.00 USD Received 18 Dec 2009; revised 19 Feb 2010; accepted 20 Feb 2010; published 24 Feb 2010

12. S. A. Prahl, "Optical properties spectra compiled by Scott Prahl" (2001), retrieved 2009, *http://omlc.ogi.edu/spectra/*.
13. C. L. Tsai, J. C. Chen, and W. J. Wang, "Near-infrared absorption property of biological soft tissue constituents," J. Med. Biol. Eng. **21**, 7–14 (2001).
14. T. J. Allen, and P. C. Beard, "Photoacoustic characterisation of vascular tissue at NIR wavelengths," Proc. SPIE **7177**, 71770A (2009).
15. F. D. Kolodgie, A. S. Katocs, Jr., E. E. Largis, S. M. Wrenn, J. F. Cornhill, E. E. Herderick, S. J. Lee, and R. Virmani, "Hypercholesterolemia in the rabbit induced by feeding graded amounts of low-level cholesterol. Methodological considerations regarding individual variability in response to dietary cholesterol and development of lesion type," Arterioscler. Thromb. Vasc. Biol. **16**(12), 1454–1464 (1996).
16. S. Kim, S. Park, S. R. Aglyamov, M. O'Donnell, and S. Y. Emelianov, "Improvement of displacement estimation using autocorrelation," Proc. International Conference on the Ultrasonic Measurement and Imaging of Tissue Elasticity, 58 (2008).
17. J. Laufer, D. Delpy, C. Elwell, and P. Beard, "Quantitative spatially resolved measurement of tissue chromophore concentrations using photoacoustic spectroscopy: application to the measurement of blood oxygenation and haemoglobin concentration," Phys. Med. Biol. **52**(1), 141–168 (2007).
18. R. R. Anderson, W. Farinelli, H. Laubach, D. Manstein, A. N. Yaroslavsky, J. Gubeli 3rd, K. Jordan, G. R. Neil, M. Shinn, W. Chandler, G. P. Williams, S. V. Benson, D. R. Douglas, and H. F. Dylla, "Selective photothermolysis of lipid-rich tissues: a free electron laser study," Lasers Surg. Med. **38**(10), 913–919 (2006).
19. S. Mallidi, T. Larson, J. Tam, P. Joshi, A. Karpiouk, K. Sokolov, and S. Emelianov, "Multiwavelength photoacoustic imaging and plasmon resonance coupling of gold nanoparticles for selective detection of cancer," Nano Lett. (2009).
20. A. B. Karpiouk, B. Wang, and S. Y. Emelianov, "Development of a catheter for combined intravascular ultrasound and photoacoustic imaging," Rev. Sci. Instrum. **81**(1), 1–7 (2010).
21. A. Roggan, M. Friebel, K. Dorschel, A. Hahn, and G. Muller, "Optical properties of circulating human blood in the wavelength range 400–2500 nm," J. Biomed. Opt. **4**(1), 36–46 (1999).

1. Introduction

Cardiovascular disease (CVD) has been the number one killer in the United States for over a century. The majority of CVD events are caused by atherosclerosis which is characterized by plaques building up inside the arterial wall [1]. Clinically, it is important to identify the vulnerable plaques, i.e., plaques that may undergo fast progression and put the patent at high risk due to possible plaque rupture leading to heart attack or stroke. There are many types of vulnerable plaques that differ based on their compositions. Since the vulnerability of the plaques is related to both plaque composition and anatomical structure, revealing the composition is critical in order to identify vulnerable plaques [2].

Lipid is an important constituent in atherosclerosis. Lipid in the plaques originates from low density lipoprotein (LDL) circulating in the blood stream. After entering the activated endothelial layer, LDL particles are endocytosed by macrophages located in the arterial wall. These LDL loaded macrophages later contribute to the lipid-rich necrotic core in the classical rupture prone plaques [3]. Moreover, it has been shown that periadventitial fat is related to vessel remodeling and inflammation in atherosclerosis [4]. Therefore, imaging lipid deposits in atherosclerotic vessels will benefit both diagnosis and understanding of the pathology of atherosclerosis.

Various imaging modalities have been used to image lipid in atherosclerotic vessels. Noninvasively, conventional magnetic resonance imaging (MRI) is capable of differentiating lipid core in the plaques, but MRI suffers from low signal-to-noise ratio (SNR) and low spatial resolution. With the help of contrast agents, nuclear imaging can also detect oxidized LDL [5]. However, similar to conventional MRI, the spatial resolution of nuclear imaging is low. Invasive imaging modalities such as intravascular MRI, intravascular ultrasound (IVUS) and optical coherence tomography (OCT) can provide higher resolution. However, none of these modalities can image with sufficient penetration depth and high sensitivity at the same time [6]. An imaging modality that can visualize the lipid in atherosclerosis with sufficient penetration depth, high resolution and high sensitivity is needed. Here we describe the utility of IVUS-guided spectroscopic intravascular photoacoustic (IVPA) imaging to assess lipid in atherosclerotic vessels.

Intravascular photoacoustic imaging is a catheter-based imaging modality capable of imaging the arterial wall [7]. After pulsed laser irradiation, the arterial tissue will emit photoacoustic signals due to differential absorption of laser energy and rapid thermal

#121713 - $15.00 USD Received 18 Dec 2009; revised 19 Feb 2010; accepted 20 Feb 2010; published 24 Feb 2010

expansion of the tissue. The amplitude of the photoacoustic signal is proportional to the wavelength-dependent optical absorption coefficient of the tissue, the local laser fluence and the Grüneisen coefficient [8]. Given the distinct optical absorption spectra of various tissue types (Fig. 1), spectroscopic IVPA imaging may be used to assess tissue composition [9]. Furthermore, using plasmonic contrast agents such as gold nanoparticles, IVPA can also image molecular and cellular events associated with atherosclerosis [10]. Finally, IVPA imaging is often combined with IVUS imaging because both imaging techniques are synergistic and share several common components such as ultrasound transducer and receiving electronics [7]. Because the same transducer is used in IVPA and IVUS imaging, spatially co-registered images can be easily acquired [7,9,10]. More importantly, by combining these two imaging modalities, functional (IVPA) and anatomical (IVUS) information about the imaged tissue can be obtained [7,11].

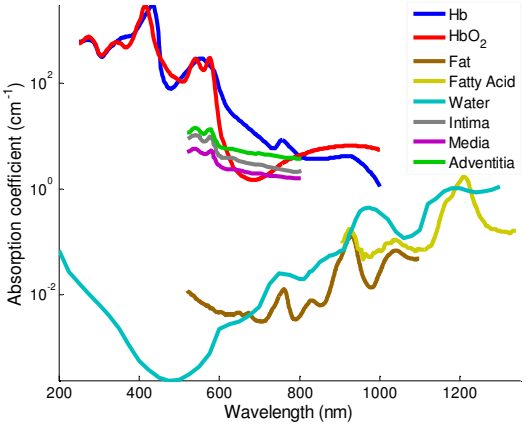

Fig. 1. Optical absorption spectra of various tissue types [12,13].

IVPA imaging is well suited for lipid detection in atherosclerosis. Because the Grüneisen coefficients of fat, lipid and oils are about two orders of magnitude higher than that of water, lipid is one of the most efficient biological media for the generation of photoacoustic transients [8]. Therefore, IVPA imaging may detect lipid with high sensitivity even though the optical absorption coefficient of lipid is lower compared to other tissue types. In the wavelength range between 1150 nm and 1250 nm, the optical absorption spectra of fatty acid and water behave differently (Fig. 1) – the optical absorption spectrum of fatty acid has a local maxima in this spectral range, while the spectrum of water is nearly constant [13]. Therefore, spectroscopic IVPA imaging of lipid may be used to differentiate lipid-rich tissue from other water-based tissues in atherosclerotic vessels [14].

In this study, the feasibility of using spectroscopic IVPA to image lipid-rich areas within the arterial wall was investigated. A bench-top IVPA imaging system was used to perform ex-vivo spectroscopic IVPA imaging of both atherosclerotic and normal arteries in the 1200–1230 nm wavelength range. To differentiate regions containing lipid deposits, an algorithm to process multi-wavelength IVPA images was developed.

2. Materials and methods

2.1 Animal model

In this study, a rabbit model of atherosclerosis was used. Specifically, a New Zealand white rabbit was kept under a 0.25% cholesterol chow for 20 months. Rabbit subject to such diet will develop advanced atherosclerosis in aorta [15]. Another rabbit kept under normal diet was used as control. After sacrificing the rabbits, aortas were removed and preserved in saline

#121713 - $15.00 USD Received 18 Dec 2009; revised 19 Feb 2010; accepted 20 Feb 2010; published 24 Feb 2010

damped gauze at 4°C. Imaging experiments were performed within 36 hours after sacrificing the rabbits.

2.2 IVUS-guided multi-wavelength IVPA imaging system

The combined IVUS/IVPA imaging system consisted of a tunable Nd:YAG pumped OPO laser capable of generating laser pulses within 680 – 950 nm and 1200 – 2400 nm spectral ranges. The laser pulse duration was 5–7 ns and the maximum wavelength-dependent fluence was 30 mJ/cm^2. A 40 MHz single element IVUS catheter (Boston Scientific, Inc.) driven by a pulser/receiver (5073PR, Olympus Inc.) was used for both ultrasound pulse-echo imaging and photoacoustic imaging. During the imaging experiment, the arterial sample was placed into a water tank and immersed in saline solution. The IVUS catheter was inserted into the lumen of aorta while the laser light was delivered by an optical fiber and irradiated the aorta from the outside (Fig. 2). The ultrasound beam of the transducer located at the tip of the IVUS imaging catheter was aligned with the laser beam from the optical fiber. A stepper motor mechanically rotated the artery for cross-sectional scanning. At each angular position, the laser light irradiated the tissue and the IVUS transducer was used to receive the photoacoustic signal. To increase signal-to-noise ratio, 8 photoacoustic signals were collected and averaged. Then, followed by a user defined delay of several microseconds, the same IVUS transducer was used to transmit and receive the ultrasound pulse-echo signal. After rotating the arterial sample 360 degrees in 256 incremental angular steps, co-registered IVPA and IVUS images of the sample were collected. Both IVUS and IVPA radio frequency signals were acquired using an A/D card (Gage, Inc.) at 200 MHz sampling rate. A power meter (Ophir, Inc.) was used to measure the energy of laser pulses at various wavelengths.

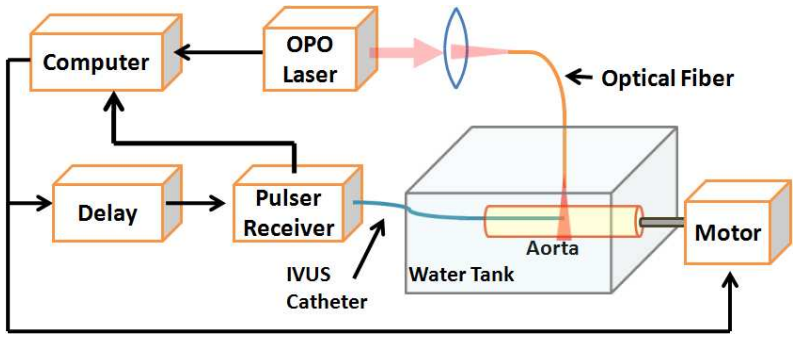

Fig. 2. IVUS-guided multi-wavelength IVPA imaging system.

2.3 Image processing

In contrast to the relatively constant optical absorption spectrum of water within 1200 – 1230 nm wavelength range, the spectrum of fatty acid decreases in this spectral range (Fig. 1). Therefore, for lipid, photoacoustic signal amplitude at 1230 nm should be lower than that at 1200 nm. We further assume that the absorption spectrum of lipid decreases nearly linearly within this wavelength range. To identify the lipid region from the multi-wavelength IVPA data, a 3-step image processing algorithm was developed.

The flowchart in Fig. 3 outlines the image processing algorithm used to analyze multi-wavelength IVPA data. To obtain cross-sectional scans at multiple wavelengths, the arterial sample was mechanically rotated several times. Consequently, the elastic arterial tissue may not return to exactly the same position from one scan to another. Therefore, the displacement of tissue between multi-wavelength scans was estimated first. Since there was a co-registered IVUS image to each IVPA scan, IVUS images with abundant anatomical information were used to estimate the tissue displacement. Suppose the spectroscopic IVPA imaging was performed at multiple wavelengths $\lambda_k \in [\lambda_1, \lambda_l], (l = 2,3,...)$, the IVUS image taken at wavelength λ_1 was then selected as the reference image, and the relative displacements of

#121713 - $15.00 USD Received 18 Dec 2009; revised 19 Feb 2010; accepted 20 Feb 2010; published 24 Feb 2010

tissue in the scans at the other wavelengths ($\lambda_2 \cdots \lambda_l$) were estimated using correlation-based motion tracking method [16]. IVPA images at other wavelengths ($\lambda_2 \cdots \lambda_l$) were then re-registered to the reference (λ_1) IVPA image to compensate for tissue motion due to inconsistent rotation of the arterial sample.

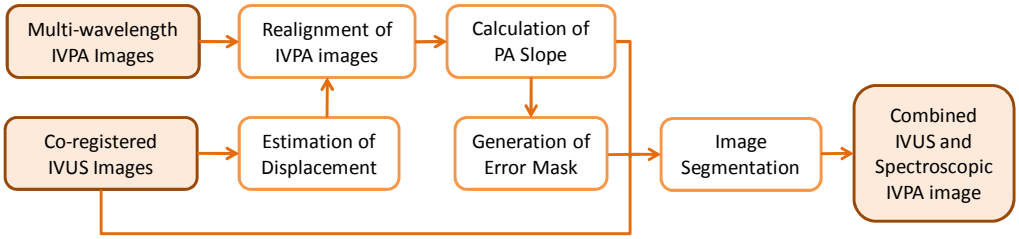

Fig. 3. Image processing algorithm for analysis of multi-wavelength IVPA and IVUS data.

In the second step, the slopes of photoacoustic signal amplitude from λ_1 to λ_l were calculated. All IVPA images were first low-pass filtered using a (m + 1) by (n + 1) moving average filter. Then, at each pixel, the slope ΔS of the photoacoustic signal amplitude was calculated and normalized to the photoacoustic signal amplitude at λ_1 wavelength:

$$\Delta S_{i,j} = \frac{1}{S_{i,j}(\lambda_1)}\left(\frac{S_{i,j}(\lambda_l) - S_{i,j}(\lambda_1)}{\lambda_l - \lambda_1}\right) \quad , \qquad (1)$$

where S is the photoacoustic signal amplitude and λ is the laser wavelength. Regions with negative slopes within a certain range were selected to indicate the potential lipid region.

In the third step, an error mask was introduced to identify regions with high level of noise based on the assumption that the photoacoustic signal amplitude should have a nearly linear decline from λ_1 to λ_l . Multi-wavelength IVPA images from λ_2 to λ_{l-1} were utilized to identify and reject large photoacoustic signal amplitude fluctuations from the linear decline with a slope of $\Delta S_{i,j}$:

$$E(i,j) = \sum_k \left| \frac{S_{i,j}(\lambda_k) - S_{i,j}(\lambda_1)}{S_{i,j}(\lambda_1)} - (\lambda_k - \lambda_1)\cdot \Delta S_{i,j} \right| \quad , \quad k = 2,3,...,l-1. \qquad (2)$$

An error $E(i, j)$ is the difference between the measured photoacoustic signal amplitude at λ_2 to λ_{l-1} and the linear fit of the photoacoustic signal amplitude between λ_1 and λ_l . The potential lipid regions defined in step two were rejected if the error E exceeded a certain value. The remaining regions were considered containing lipid.

For display purposes, tissue boundaries, identified from the IVUS image taken during the IVPA scan at λ_1 wavelength, were used to segment the spectroscopic IVPA image. Furthermore, because the images were acquired and processed in the polar system of coordinates, the IVUS and the spectroscopic IVPA images were scan converted to Cartesian grid and displayed using logarithmic scale.

In this study, the tissue sample was imaged every 10 nm within 1200–1230 nm wavelength range. A kernel measuring 79 μm axially (21 samples) and 7 degrees azimuthally (5 beams) was used for low-pass filtering. Potential lipid regions were identified using negative slopes in the range from –0.02/nm to –0.007/nm (Eq. (2)). An error threshold of 40% was used to reject regions with large fluctuations of the slope.

#121713 - $15.00 USD Received 18 Dec 2009; revised 19 Feb 2010; accepted 20 Feb 2010; published 24 Feb 2010

3. Results

The cross-sectional IVUS, 1200-nm IVPA and combined IVUS/IVPA images of the diseased and normal (i.e., control) rabbit aortas are shown in Fig. 4. All images cover 7.5 mm diameter areas. The IVUS images (Figs. 4(a) and 4(d)) clearly demonstrate the structure of the vessels. Thickened intima layer in the diseased aorta corresponds to the hypoechoic regions in the IVUS image (Fig. 4(a)). Combined IVUS/IVPA images (Figs. 4(c) and 4(f)) highlight the amplitude and location of photoacoustic signals in relation to the arterial anatomy. Because the artery was irradiated externally, higher laser fluence at the outer boundary of the artery resulted in higher photoacoustic response. Notice that despite the exponential decline of laser fluence with imaging depth, photoacoustic signals with relatively high amplitude were detected in the thickened intima layer of the diseased aorta.

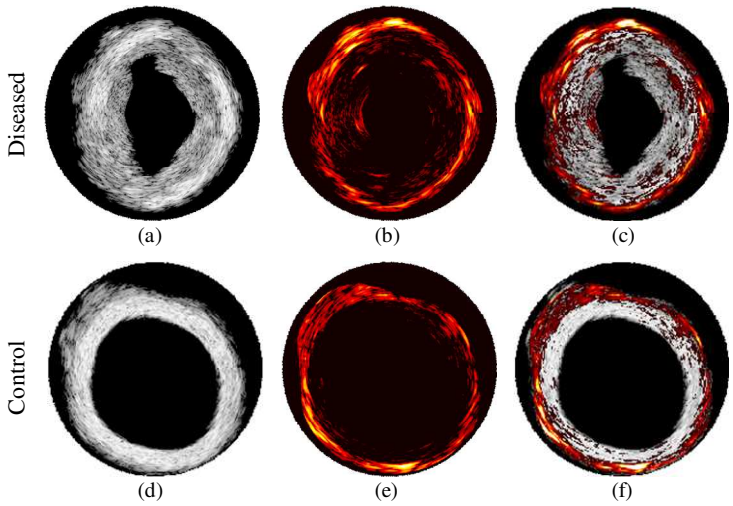

Fig. 4. Cross-sectional (a,d) IVUS, (b,e) 1200-nm IVPA, and (c,f) combined IVUS/IVPA images of the diseased and normal aorta. The IVUS and IVPA images are displayed using 40 dB dynamic range.

The multi-wavelength photoacoustic response from several representative regions of the aortas are presented in Fig. 5. Specifically, a photoacoustic response in the thickened intima (region 1, Fig. 5(a)) is compared with that in the media-adventitia of both the diseased (region 2, Fig. 5(a)) and normal aorta (region 3, Fig. 5(b)). The signal amplitude in region 1 monotonically decreases with increased wavelength (Fig. 5(c)). This decreasing trend corresponds to the absorption spectrum of fatty acid (Fig. 1). Therefore, we assumed that photoacoustic signals in region 1 were generated from the lipid-rich areas. In contrast, photoacoustic signal amplitudes from the media-adventitia of both the diseased and normal aorta remain relatively constant – such photoacoustic response in this spectral region closely corresponds to the optical absorption spectrum of water-based tissues. Therefore, lipid-rich regions in atherosclerotic vessels may be detected by analyzing the multi-wavelength photoacoustic signal, e.g. by differentiating areas with different spectral behavior of multi-wavelength photoacoustic signals.

#121713 - $15.00 USD Received 18 Dec 2009; revised 19 Feb 2010; accepted 20 Feb 2010; published 24 Feb 2010

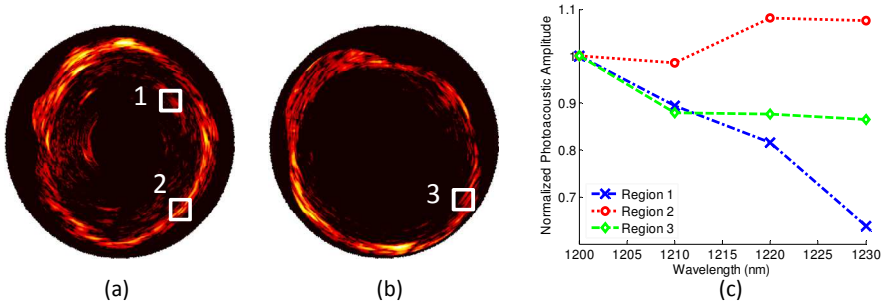

Fig. 5. Cross-sectional IVPA images of (a) diseased and (b) normal aortas obtained using 1200 nm wavelength. (c) Comparison of the wavelength-dependent photoacoustic responses from the lipid-rich area of the atherosclerotic plaque (region 1) and media-adventitial layer of diseased (region 2) and normal (region 3) aortas.

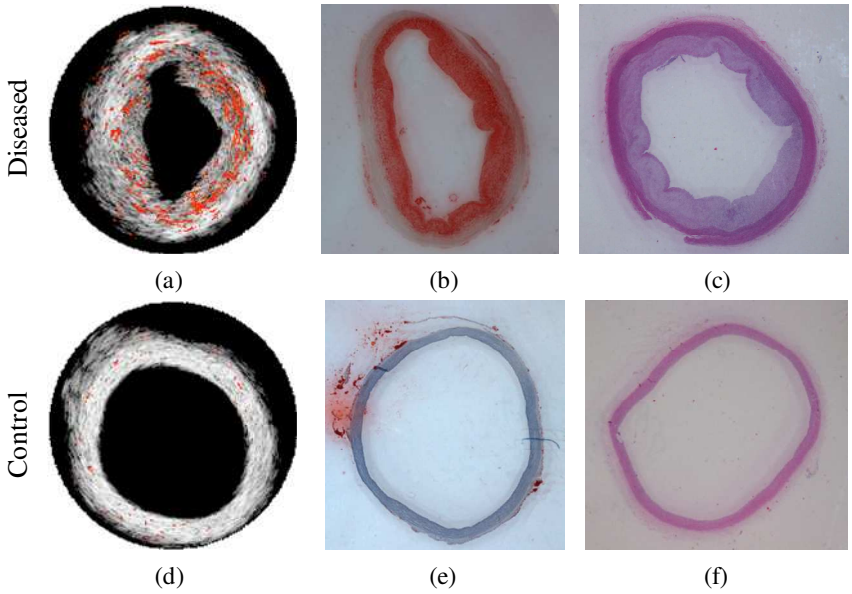

Fig. 6. Combined IVUS and spectroscopic IVPA images and corresponding histological slices of the diseased atherosclerotic aorta (a-c) and normal (i.e., control) aorta (d-e). Lipid-rich regions (orange color) were identified from multi-wavelength photoacoustic imaging and displayed over the IVUS images. Lipid-rich regions were detected in the thickened intima layer of the diseased aorta (a) confirmed by Oil red O stain for lipid (b) and H&E stain (c). In contrast, spectroscopic IVPA imaging (d) and tissue histology (e and f) show insignificant lipid-rich regions in normal rabbit aorta. Both normal and diseased aortas show some insignificant deposits of lipid in the periadventitia.

Given the differences in tissue type-dependent spectral behavior of photoacoustic signals, analysis of multi-wavelength IVPA images was performed to identify regions with enhanced content of lipid. The lipid-rich regions, i.e. regions with anticipated spectroscopic behavior of IVPA signals (Fig. 5), were color-coded and plotted over co-registered IVUS images (Fig. 6(a) and Fig. 6(d)). Clearly, lipid-rich regions were detected in the thickened intima of the diseased aorta but no significant lipid-rich regions were present in normal aorta. The location of lipid-rich areas was further confirmed by examination of tissue cross-sections adjacent to the imaged location. Both the Oil red O stain for lipid (Fig. 6(b)) and H&E stain (Fig. 6(c)) show that the plaques in the diseased aorta are lipid-rich, whereas no lipid was present in the intima of the normal aorta (Figs. 6(e) and Fig. 6(f)). Both normal and diseased aortas show some lipid in the periadventia but this is unrelated to atherosclerosis. The Oil red O stain of

#121713 - $15.00 USD Received 18 Dec 2009; revised 19 Feb 2010; accepted 20 Feb 2010; published 24 Feb 2010

the diseased aorta shows diffuse distribution of the lipid deposits. Similar scattered distribution of lipid is reflected in the spectroscopic IVPA image (Fig. 6(a)). These results suggest that spectroscopic IVPA imaging may be used to identify the lipid-rich regions in atherosclerotic vessels.

4. Discussion and conclusion

To quantitatively evaluate the optical absorption property of tissue based on the photoacoustic response, wavelength dependent optical properties of tissues need to be taken into account [17]. In this study, a narrow wavelength range of 1200–1230 nm was used for IVPA imaging to minimize the effect of wavelength-dependent optical properties on the spectroscopic IVPA data analysis. The narrow imaging wavelength range benefited the spectroscopic analysis in two ways. First, the limited range of IVPA imaging wavelength guaranteed the nearly linear decline of the photoacoustic signal from lipid-rich regions within 1200–1230 nm. Second, the effect of wavelength-dependent laser fluence distribution was minimal and thus did not affect significantly the relative changes of photoacoustic signal amplitude.

The photoacoustic response of the suspected lipid-rich region in the diseased aorta followed a monotonic decrease in the 1200–1230 nm range (region 1 in Fig. 5). However, other researchers have found that fatty acid, pork lard and human fat have an absorption peak at around 1210 nm wavelength [13,18]. The discrepancy between multi-wavelength photoacoustic signal amplitude and the optical absorption spectrum of lipid may be due to several factors including the wavelength dependent fluence distribution in the tissue, the spectral line width of the laser source, the mixture of lipid and other tissue types in the intima of the diseased aorta, the small inaccuracy in the reported wavelength of our OPO laser, and the differences in absorption spectrum between fatty acid and lipid in plaques. To capture the peak absorption of the lipid, the artery should be imaged within, for example, 1170–1230 nm range to include anticipated peak absorption – our pulsed laser system was operating at the spectral edge of its idler mode (1200 nm to 2400 nm) and did not allow such measurements. However, if the measurements are performed around the peak optical absorption of tissue, other correlation based methods, e.g. intraclass correlation analysis [19], may provide better sensitivity than the slope-based method. Nevertheless, the slope-based method is computationally efficient and is less sensitive to the shift or shape change of the measured photoacoustic signal peak caused by wavelength dependent optical properties. The slope-based algorithm only requires imaging at several wavelengths thus shortening the imaging time and reducing the complexity of image processing. In comparison, the correlation-based methods may require measurements covering a broader range of wavelengths and resulting in larger data sets.

The parameters of the slope-based spectroscopic analysis were selected based on the optical absorption spectrum of fatty acid. After the peak absorption at 1210 nm wavelength, the absorption coefficient of fatty acid drops 60% as the wavelength increases to 1230 nm. Considering the smoothing effect of spectral line width of the laser source, we selected the slopes ranging between –0.02/nm to –0.007/nm to represent lipid-rich areas. Given the wavelength dependent fluence distribution and laser pulse energy variation, we used a 20% error per wavelength to tolerate the change in the photoacoustic signal amplitude.

The false positive signals in the normal aorta and the media-adventitial layer of the diseased aorta may be due to inaccuracies in tissue displacement estimation due to out-of-plane motion during mechanical rotation of the tissue sample. The normal aorta was more likely subject to this type of artifact because it was more flexible compared to the diseased aorta characterized by a thick vessel wall. However, compensation for tissue motion may become even more critical in spectroscopic IVPA imaging in-vivo because cardiac motion will introduce tissue displacement between multi-wavelength IVPA scans.

The sensitivity and specificity of our measurements were affected by the laser system and the limited knowledge of optical properties of arterial tissue. Because the OPO laser was operating at the spectral edge of its idler mode, the line width of the laser pulse was around 10 nm. Such broad line width may reduce the sensitivity for imaging lipid which has a sharp

#121713 - $15.00 USD Received 18 Dec 2009; revised 19 Feb 2010; accepted 20 Feb 2010; published 24 Feb 2010

absorption peak. Using a laser with narrower spectral line width may increase the sensitivity and reduce the required laser energy to detect lipid-rich regions in the vessels. Because of limited available measurements of optical spectra of different tissue types in the wavelength around 1200 nm, we generally classify tissues into two categories: lipid-rich tissues or water-based tissues. Knowledge of the absorption spectra of lipid and other tissue will improve the specificity of identifying lipid-rich regions.

Using integrated IVUS/IVPA catheter, high sensitivity and high resolution spectroscopic IVPA imaging in-vivo is possible [20]. Indeed, the low optical scattering of blood and arterial tissue around 1200 nm wavelength ensures sufficient penetration depth in IVPA imaging [21]. The higher threshold of the maximum permissible exposure at this wavelength range reduces the concern of laser thermal damage. Moreover, IVPA imaging with high frequency IVUS transducer can achieve axial resolution of tens of micrometers. Since modest low-pass filtering was applied in spectroscopic IVPA imaging, the axial resolution of the spectroscopic IVPA image is decreased by 2-3 times compared to the axial resolution of the IVPA image alone.

In the future, quantitative studies will be performed to examine the agreement between lipid-rich regions identified from spectroscopic IVPA and histological stain. Furthermore, human atherosclerotic lesions tend to have more complex plaques. Therefore, the performance of spectroscopic IVPA to differentiate various tissue types including lipid needs to be studied.

In conclusion, a method to differentiate lipid-rich regions in atherosclerotic vessels using spectroscopic IVPA imaging together with IVUS imaging was introduced. Ex-vivo tissue studies demonstrated that the spectroscopic IVPA imaging in the 1200-1230 nm wavelength range can successfully identify lipid-rich regions in the atherosclerotic rabbit aorta. Generally, spectroscopic IVPA imaging has the potential to identify tissue composition based on intrinsic optical absorption contrast between various types of tissues.

Acknowledgements

This work was supported in part by the National Institutes of Health under grant HL096981. The authors would like to acknowledge the technical support from Boston Scientific, Inc.

#121713 - $15.00 USD Received 18 Dec 2009; revised 19 Feb 2010; accepted 20 Feb 2010; published 24 Feb 2010